Latin American Journal of Solids and Structures
www.lajss.org

Analytical Couple-stress Solution for Size-dependent Large-amplitude Vibrations of FG Tapered-nanobeams

Abstract

In this paper, analytical couple-stress solution for size-dependent large-amplitude vibrations of FG (functionally-graded) tapered-nanobeams is presented. Using the modified couple-stress theory, the small scale effects are accounted for. Employing the Homotopy-Pade Analysis Method, efficient and accurate analytical expressions for the deflection and non-linear frequencies of the both single and double tapered nanobeam are presented. Very good agreement is observed between the present work results and some available results reported in the literature. This study may be helpful to investigate the size-dependent mechanical properties of MEMS\NEMS. Therefore, the proposed analytical solution can be used as an efficient tool for the material or geometrical parametric studies of small scale devices consisting of beams for their design and optimization which involves a large number of simulations.

Keywords

Size dependent, couple-stress theory, functionally-graded, tapered beams, large amplitude, Homotopy-Pade Analysis method.

M. Baghani [a*]
M. MohammadSalehi [b]
P. H.Dabaghian [c]

[a] School of Mechanical Engineering, College of Engineering, University of Tehran, P. O. Box 11155-4563, Tehran, Iran
* Corresponding Author
baghani@ut.ac.ir
[b] School of Mechanical Engineering, College of Engineering, University of Tehran, Tehran, Iran ammsalehi@ut.ac.ir
[c] Railway Engineering Department, Iran University of Science and Technology, Tehran, Iran
pedram.hd@gmail.com

http://dx.doi.org/10.1590/1679-78252175

Received 30.05.2015
In Revised Form 11.09.2015
Accepted 15.09.2015
Available online 22.09.2015

1 INTRODUCTION

Micro/nano-scale mechanical structures are structures whose characteristic size is in the order of micron or submicrons, e.g., micro/nano-beams and micro/nano-cylinders. These elements are widely used in micro- and nano-electromechanical devices (MEMS and NEMS) (Baghani, 2012; Sadeghi et al., 2012; Koochi et al., 2014; Rezaiee-Pajand and Yaghoobi, 2014). Micro/nano-scale mechanical elements are also used in micro-pumps, accelerometers, micro-mirrors and microswitches. A large number of engineering applications utilize the mechanical properties of thin films materials for tar-

geted performance specifications such as those vibration shock sensor, atomic force microscopes and resonant testing method (Kong et al., 2008).

Functionally gradient materials (FGMs) utilized in e.g., space devices are high-performance heat-resistant materials which are able to tolerate extremely large temperature gradients (Koizumi and Niino, 1995; Ansari et al., 2014). Meanwhile, FGM concepts have triggered world-wide research activities which are applied to metals, ceramics and organic composites to produce modified components with superior physical and mechanical properties (Schulz et al., 2003). In recent years, the application of FGMs has broadly been spread in micro and nano structures such as thin films in the form of shape memory alloys (Fu et al., 2003, 2004) and also in MEMS and NEMS (Witvrouw and Mehta, 2005; Lee et al., 2006). In addition to FG functionality, especially in beams, changes in the cross-section (gradually or abruptly along the length) could also play an important role in different engineering fields as a design tool. They are used in optimization of the structures' weight and strength, as well as in architectural and aesthetical aspects of structural engineering design. These particular features enable the engineers to design and construct precise structures, e.g., aerospace structures.

There are several experimental evidences which reveal that the behavior of micro-structures is size dependent (Fleck et al., 1994; Lam et al., 2003; McFarland and Colton, 2005; Stolken and Evans, 1998). Lam et al. (2003) observed that during the bending test of epoxy polymeric micro-beams the normalized bending rigidity of the beams becomes 2.4 times larger when the thickness of the beam reduces from 115 μm to 20 μm. McFarland and Colton (2005) have experimentally investigated the bending of polypropylene small-sized cantilever beams. They observed that the stiffness of the small-sized cantilevers was at least 4 times larger than the value which the classical theory of elasticity anticipated. To properly predict the behavior of such structures, non-classical theories such as couple-stress theory, nonlocal elasticity, Cosserat continuum and strain gradient elasticity have been developed to take into account the size-dependent materials' behavior in small-scales (Mindlin and Eshel, 1968; Yang et al., 2002; Yoshiyuki, 1968).

MEMS/NEMS systems' responses have been the subject of several analytical studies in two past decades. Based on the modified couple-stress theory introduced by Yang et al. (2002), Kong et al. (2008) analytically calculated the size-dependent natural frequencies of Euler-Bernoulli beams. Shahba et al. (2011) studied the free vibration and stability analysis of axially FG tapered Timoshenko beams using a finite element approach. There are also several numerical investigations about different aspects of vibration of tapered beams (see e.g., Cheng et al. (2011); Saffari et al. (2008); Bazoune et al. (2001) among others). Baghani (2012) have analytically studied the deflection and static pull-in voltage of cantilevers based on the modified couple-stress theory. It has been shown that the couple-stress theory can successfully remove the gap between the experimental observations and the classical theory based simulations for the static pull-in voltage. Ke and Wang (2011) have studied the size effect on dynamic stability of FG microbeams based on a modified couple stress theory. They have also investigated on nonlinear free vibration of size-dependent functionally graded microbeams (Ke et al., (2012)).

It is noted that the governing equations of such systems are essentially non-linear. Generally in a non-linear problem, it is hard to arrive at an analytical solution unless numbers of different simplifying assumptions are considered. Otherwise, application of different numerical techniques is una-

voidable (Baghani et al., 2011, 2012). However, it is difficult to arrive at an indispensable understanding of a non-linear problem out of the numerical results. Further, numerical complications may occur, if a non-linear problem contain singularities or multiple solutions. Among different analytical methods, the Homotopy Perturbation Method (HPM) is one of the most accurate and efficient methods for studying non-linear systems (Liao, 2004, 2003).

In this paper, employing the modified couple-stress theory, the size-dependent non-linear vibration of FG tapered Euler-Bernoulli beams is analytically investigated. Incorporating the inextensibility condition in the model, a kinematic dependency between axial and transverse displacements is produced. Analytical expressions for the deflection of these beams are obtained using the HAM. The impact of FG parameters and also size-dependent effects on the non-linear response of beams are analytically studied. Finally, results are compared with experimental data as well as the numerical results available from the literature.

2 GOVERNING EQUATIONS BASED ON THE MODIFIED COUPLE-STRESS THEORY

In the modified couple-stress theory, the strain energy density for an elastic material in the infinitesimal deformation is introduced as (Yang et al., 2002; Asghari et al., 2011)[1]:

$$\bar{U} = 1/2\left(\boldsymbol{\sigma} : \boldsymbol{\varepsilon} + \mathbf{m} : \boldsymbol{\chi}\right) \tag{1}$$

In especial isotropic case, we may write:

$$\boldsymbol{\varepsilon} = 1/2\left(\nabla\mathbf{u} + \nabla\mathbf{u}^T\right) \tag{2}$$

$$\boldsymbol{\sigma} = \lambda\,\mathrm{tr}\left(\boldsymbol{\varepsilon}\right)\mathbf{1} + 2\mu\boldsymbol{\varepsilon} \tag{3}$$

$$\boldsymbol{\chi} = 1/2\left(\nabla\boldsymbol{\theta} + \nabla\boldsymbol{\theta}^T\right); \qquad \boldsymbol{\theta} = 1/2\,\mathrm{curl}\left(\mathbf{u}\right) \tag{4}$$

$$\mathbf{m} = 2l^2\mu\boldsymbol{\chi} \tag{5}$$

where $\mathbf{u}$ and $\boldsymbol{\theta}$ are the displacement and rotation vectors, respectively. Also $\boldsymbol{\varepsilon},\boldsymbol{\sigma},\mathbf{m}$ and $\boldsymbol{\chi}$ stand for strain, stress, couple stress and curvature tensors, respectively. The material length scale parameter is represented by l, while λ and μ are Lame' constants.

We now consider a FG tapered beam (shown in Figure 1). The axial and transverse components of the displacement vector are:

$$u_x = u\left(x,t\right) - z\frac{\partial w\left(x,t\right)}{\partial x};\; u_y = 0;\; u_z = w\left(x,t\right) \tag{6}$$

in which u_x, u_y and u_z are the displacement components. It is assumed that all cross sections remain plane after deformation; but, they can experience a rigid body displacement in xz plane

[1]Double contraction between second order tensors **A** and **B** denoted by : is defined as $\mathbf{A} : \mathbf{B} = A_{ij}B_{ij}$; (i, j = 1..3)

and/or a rotation about y-axis. Assuming small slopes after deformation but finite deflection w, the axial strain can be approximately calculated by the von-Karman strain as:

$$\varepsilon_{xx} = \frac{\partial u}{\partial x} - z\frac{\partial^2 w}{\partial x^2} + \frac{1}{2}\left(\frac{\partial w}{\partial x}\right)^2 \tag{7}$$

In view of equations (2-5), we obtain:

$$\theta_x = 0; \quad \theta_y = -\frac{\partial w(x,t)}{\partial x}; \quad \theta_z = 0 \tag{8}$$

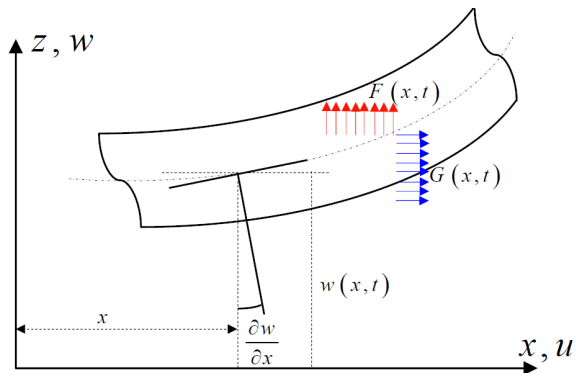

Figure 1: An Euler-Bernoulli, loading and coordinate system.

Substitution of (8) in to (4) gives $\chi_{xy} = -\partial^2 w/\partial x^2$ while other components vanish. Therefore, non-zero components of the stress and couple-stress tensors are easily found as follows:

$$\begin{cases} \sigma_{xx} = E\left(\dfrac{\partial u}{\partial x} - z\dfrac{\partial^2 w}{\partial x^2} + \dfrac{1}{2}\left(\dfrac{\partial w}{\partial x}\right)^2\right) \\ m_{xy} = -\mu l^2 \dfrac{\partial^2 w}{\partial x^2} \end{cases} \tag{9}$$

To obtain the governing equations, the kinetic energy of the beam T and the beam strain energy U are considered as follows:

$$T = \frac{1}{2}\int_0^L \rho\left[A\dot{u}^2 + I\dot{w}'^2 + A\dot{w}^2\right]\mathrm{d}x \tag{10}$$

$$U = \frac{1}{2}\int_0^L \left\{ \overbrace{EA\left(u' + \frac{1}{2}w'^2\right)^2 + \left(EI + \mu A l^2\right)w''^2}^{\text{Beam strain energy due to bending}} + \overbrace{N_0\left(2u' + w'^2\right)}^{\text{Beam strain energy due to existence of initially axial load } N_0} \right\}\mathrm{d}x \tag{11}$$

where A, I, L and N_0 is the cross-sectional area, the second moment of inertia of the cross-section about the y-axis, beam length and the initial axial load, respectively. E and ρ are also the effective Young's modulus and density, respectively. The strain energy is composed of two parts: first part due to bending and also due to the change of the stretch with respect to the initial configuration, and second part the increase in the stored energy with respect to the initial configuration due to the existence of initially axial load N_0. It is noted that the x-axis lies on the neutral-axis of the beam ($\int_A z\,\mathrm{d}A = 0$).

To derive the governing equations of motion of the FG tapered beam, the Hamilton principle is utilized as:

$$\int_{t_1}^{t_2}\left\{-\delta T+\delta U-\delta W\right\}\mathrm{d}t=0 \tag{12}$$

After some mathematical manipulations (integral by parts, ...), we arrive at:

$$\begin{aligned}&\int_{t_1}^{t_2}\delta T\,\mathrm{d}t=-\int_{t_1}^{t_2}\int_0^L\rho\left[A\ddot{u}\delta u+\left(A\ddot{w}-\left[I\ddot{w}'\right]'\right)\delta w\right]\mathrm{d}x\,\mathrm{d}t\\&+\int_0^L\rho\left[A\dot{u}\delta u+I\dot{w}'\delta w'+A\dot{w}\delta w\right]\mathrm{d}x\Big|_{t_1}^{t_2}-\int_{t_1}^{t_2}\rho I\ddot{w}'\delta w\,\mathrm{d}t\Big|_{x=0,L}\end{aligned} \tag{13}$$

And

$$\begin{aligned}&\int_{t_1}^{t_2}\delta U\,\mathrm{d}t=\int_{t_1}^{t_2}\left\{\left[EA\left(u'+\frac{1}{2}w'^2\right)+N_0\right]w'\delta w\right\}\mathrm{d}t\Big|_{x=0,L}\\&-\int_{t_1}^{t_2}\int_0^L\left\{\left[EA\left(u'+\frac{1}{2}w'^2\right)+N_0\right]'w'+\left[EA\left(u'+\frac{1}{2}w'^2\right)+N_0\right]w''\right\}\delta w\,\mathrm{d}x\,\mathrm{d}t\\&+\int_{t_1}^{t_2}\left[\left(EI+\mu Al^2\right)w''\delta w'-\left(w''\left(EI+\mu Al^2\right)\right)'\delta w\right]\mathrm{d}t\Big|_{x=0}^{L}+\int_{t_1}^{t_2}\int_0^L\left(\left(EI+\mu Al^2\right)w''\right)''\delta w\,\mathrm{d}x\,\mathrm{d}t\\&-\int_{t_1}^{t_2}\int_0^L\left[EA\left(u'+\frac{1}{2}w'^2\right)+N_0\right]'\delta u\,\mathrm{d}x\,\mathrm{d}t+\int_{t_1}^{t_2}\left[EA\left(u'+\frac{1}{2}w'^2\right)+N_0\right]\delta u\mathrm{d}t\Big|_{x=0}^{L}\end{aligned} \tag{14}$$

In addition, the virtual work done by external loads are expressed as:

$$\delta W=\int_0^L F\left(x,t\right)\delta w\mathrm{d}x+\int_0^L G\left(x,t\right)\delta u\mathrm{d}x+\left[\bar{M}\delta w'+\bar{V}\delta w+\bar{N}\delta u\right]\Big|_{x=0,L} \tag{15}$$

in which $G\left(x,t\right)$ and $F\left(x,t\right)$ are body forces along x and y axes, respectively. The external transverse force, the axial force and the total moment acting on the beam ends are expressed by $\bar{V}$, $\bar{N}$ and $\bar{M}$, respectively.

Finally, substitution of (13), (14) and (15) into (12) and equating coefficients of similar variations, we obtain:

$$\begin{aligned}
&\delta u: \quad \rho A\ddot{u} = \left[EA\left(u' + \frac{1}{2}w'^2\right) + N_0\right]' + G\left(x,t\right) \\
&\left[EA\left(u' + \frac{1}{2}w'^2\right) + N_0 - \bar{N}\right]\Big|_{x=0,L} = 0 \ \text{ or } \ \delta u\big|_{x=0,L} = 0
\end{aligned} \tag{16}$$

$$\begin{aligned}
&\delta w: \ \left(\left(EI + \mu A l^2\right)w''\right)'' - \left(\left[EA\left(u' + \frac{1}{2}w'^2\right) + N_0\right]w'\right)' + \rho A\ddot{w} - \left[\rho I\ddot{w}'\right]' = F\left(x,t\right) \\
&\left[\left[EA\left(u' + \frac{1}{2}w'^2\right) + N_0\right]w' - \left(\left(EI + \mu A l^2\right)w''\right)' - \bar{V} + \rho I\ddot{w}'\right]\Big|_{x=0,L} = 0 \ \text{ or } \ \delta w\big|_{x=0,L} = 0
\end{aligned} \tag{17}$$

$$\delta w': \quad \left(EI + \mu A l^2\right)w'' - \bar{M}\big|_{x=0,L} = 0 \tag{18}$$

In the following sections, we focus on analytical solution of set of equations (16-18).

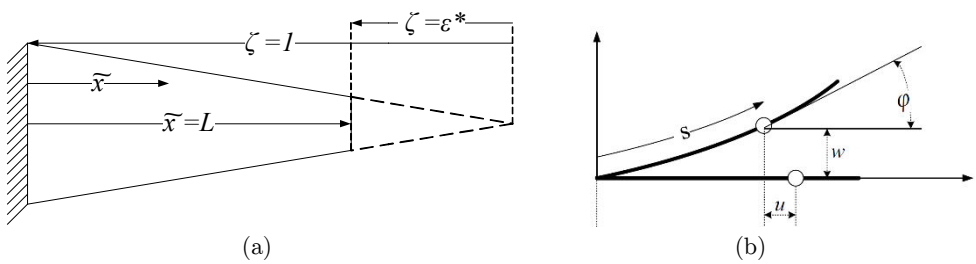

Figure 2: a: Initial configuration of the FG tapered nanobeam. b: Deflection of the neutral axis.

3 INEXTENSIBILITY CONDITION

Consider the FG tapered micro-cantilever beam as illustrated in Figure 2, where $\tilde{x} = x / L$ and κ is the curvature of the beam neutral axis. ζ is a dimensionless parameter which varies from ε^* (free end) to 1 (clamped end). Applying the change of parameter $w' = \sin\varphi$ (prime represents the derivative with respect to x) and using the fact that $\kappa = \varphi'$, it is concluded that:

$$\varphi' = \frac{w''}{\sqrt{1 - w'^2}} \tag{19}$$

Applying the Taylor series to (19), we may write:

$$\varphi' = w''\left(1 + 1 / 2w'^2\right) \tag{20}$$

Considering the relation $\kappa = \varphi'$, we derive an explicit form for the beam curvature as:

$$\kappa^2 = w''^2\left(1 + w'^2 + 1/4w'^4\right) \tag{21}$$

The inextensibility condition in special case of $w' << 1$ leads to the following relation for the axial displacement u (Abdel-Jaber et al., 2008; Al-Qaisia and Hamdan, 1999):

$$u = 1/2 \int_0^x \left(w'^2 + 1/4 w'^4 \right) dx \tag{22}$$

Differentiating the relation (22) with respect to x gives:

$$u' = 1/2 \left(w'^2 + 1/4 w'^4 \right) \tag{23}$$

Substituting (23) into (17), we may write:

$$\left(\left(EI + \mu A l^2 \right) w'' \right)'' - \left(EA \left(w'^3 + \frac{1}{8} w'^5 \right) + N_0 w' \right)' + \rho A \ddot{w} - \left[\rho I \ddot{w}' \right]' = F(x,t) \tag{24}$$

with the following boundary conditions:

$$\begin{cases} \left[EA \left(w'^3 + \frac{1}{8} w'^5 \right) + N_0 w' - \left(\left(EI + \mu A l^2 \right) w'' \right)' - \bar{V} + \rho I \ddot{w}' \right] \Big|_{x=0,L} = 0 \text{ or } \delta w \big|_{x=0,L} = 0 \\ \left(EI + \mu A l^2 \right) w'' - \bar{M} \big|_{x=0,L} = 0 \text{ or } \delta w' \big|_{x=0,L} = 0 \end{cases} \tag{25}$$

Introducing the dimensionless parameters,

$$\begin{cases} \tau = \beta t; \quad \tilde{x} = \frac{x}{L}; \quad \tilde{w} = \frac{w}{h_0}; \quad \tilde{l} = \frac{l}{L}; \quad \chi = \frac{h_0}{L}; \quad \tilde{A} = \frac{A}{L^2}; \quad \tilde{I} = \frac{I}{L^4} \\ \tilde{\rho} = \frac{\rho}{\rho_0}; \quad \tilde{E} = \frac{E}{E_0}; \quad \tilde{\mu} = \frac{\mu}{E_0}; \quad \tilde{\nu} = \frac{\nu}{\nu_0}; \quad \tilde{\kappa} = \frac{\rho_0 L^2 \beta^2}{E_0} \\ \tilde{N}_0 = \frac{N_0}{E_0 L^2}; \quad \tilde{\bar{V}} = \frac{\bar{V}}{E_0 h_0 L}; \quad \tilde{\bar{M}} = \frac{1}{E_0 h_0 L^2} \bar{M}; \quad \tilde{F}(\tilde{x},\tau) = \frac{F(x,t)}{E_0 h_0} \end{cases} \tag{26}$$

the governing equations are represented as follows:

$$\left(\left(\tilde{E}\tilde{I} + \tilde{\mu}\tilde{A}\tilde{l}^2 \right) \tilde{w}'' \right)'' - \left(\tilde{E}\tilde{A} \left(\chi^2 \tilde{w}'^3 + \frac{1}{8} \chi^4 \tilde{w}'^5 \right) + \tilde{N}_0 \tilde{w}' \right)' + \tilde{\kappa} \left(\tilde{\rho}\tilde{A} \overset{\circ\circ}{\tilde{w}} - \left[\tilde{\rho}\tilde{I} \overset{\circ\circ}{\tilde{w}}' \right]' \right) = \tilde{F}(\tilde{x},\tau) \tag{27}$$

$$\begin{cases} \left[\tilde{E}\tilde{A} \left(\chi^2 \tilde{w}'^3 + \frac{1}{8} \chi^4 \tilde{w}'^5 \right) + \tilde{N}_0 \tilde{w}' - \left(\left(\tilde{E}\tilde{I} + \tilde{\mu}\tilde{A}\tilde{l}^2 \right) \tilde{w}'' \right)' - \tilde{\bar{V}} + \tilde{\kappa}\tilde{\rho}\tilde{I} \overset{\circ\circ}{\tilde{w}}' \right] \Big|_{\tilde{x}=0,1} = 0 \text{ or } \delta \tilde{w} \big|_{x=0,1} = 0 \\ \left(\tilde{E}\tilde{I} + \tilde{\mu}\tilde{A}\tilde{l}^2 \right) \tilde{w}'' - \tilde{\bar{M}} \big|_{\tilde{x}=0,1} = 0 \text{ or } \delta w' = 0 \end{cases} \tag{28}$$

where $\circ$ denotes the derivative with respect to $\hat{t}$. In order to account for functionality of the material parameters, the following forms are used for the density, elastic modulus and Poisson's ratio:

$$\begin{cases} \tilde{\rho} = 1 + \left(\rho_1/\rho_0 - 1\right)\tilde{x}^n; \quad \tilde{E} = 1 + \left(E_1/E_0 - 1\right)\tilde{x}^m; \quad \nu = \nu_0 + \left(\nu_1 - \nu_0\right)\tilde{x}^p \\ \tilde{\mu} = \dfrac{\mu}{E_0} = \dfrac{E/E_0}{2\left(1+\nu\right)} = \dfrac{1 + \left(E_1/E_0 - 1\right)\tilde{x}^m}{2\left(1 + \nu_0 + \left(\nu_1 - \nu_0\right)\tilde{x}^p\right)} \end{cases} \tag{29}$$

in which $\rho_0, \rho_1, E_0, E_1, \nu_0, \nu_1, n, m$ and p are material parameters. In this work, we focus on the solution of the system under a single active mode. Therefore, a preferred single mode method is used in the following form:

$$\tilde{w}\left(\tilde{x}, \hat{t}\right) = \psi\left(\tilde{x}\right) q\left(\hat{t}\right) \tag{30}$$

where $\psi\left(\tilde{x}\right)$ is the dominant assumed mode while $q\left(\hat{t}\right)$ stands for the time dependency of the transverse displacement $\tilde{w}\left(\tilde{x}, \hat{t}\right)$. Multiplying equation (28) by $\psi\left(\tilde{x}\right)$ and integrating along the x-axis, the governing equation of motion is calculated as:

$$\overset{\circ\circ}{q} + c_2\, q + c_4 q^3 + c_5 q^5 = f\left(\hat{t}\right) \tag{31}$$

where

$$\begin{cases} c_1 = \tilde{\kappa}\displaystyle\int_0^1 \psi\left(\tilde{\rho}\tilde{A}\psi - \left[\tilde{\rho}\tilde{I}\psi'\right]'\right)\mathrm{d}\tilde{x} \\ c_2 = \dfrac{1}{c_1}\displaystyle\int_0^1 \psi\left[\left(\left(\tilde{E}\tilde{I} + \tilde{\mu}\tilde{A}\tilde{l}^2\right)\psi''\right)'' - \left(\tilde{N}_0\psi'\right)'\right]\mathrm{d}\tilde{x} \\ c_4 = \dfrac{-\chi^2}{c_1}\displaystyle\int_0^1 \psi\left(\tilde{E}\tilde{A}\psi'^3\right)'\mathrm{d}\tilde{x};\ c_5 = \dfrac{-\chi^4}{8c_1}\int_0^1 \psi\left(\tilde{E}\tilde{A}\psi'^5\right)'\mathrm{d}\tilde{x} \end{cases} \tag{32}$$

The beam neutral axis is subjected to the following initial conditions:

$$\overset{\circ}{\tilde{w}}\left(1,0\right) = \tilde{a}, \qquad \overset{\circ}{q}\left(0\right) = 0 \tag{33}$$

where $\tilde{a}$ is the initial amplitude of beam deflection at the free end. Mode shape amplitudes are normalized in such a way that they satisfy the relation $\psi\left(1\right) = 1$. This assumption gives $q\left(0\right) = \tilde{a}$.

It is also from (33) obtained that $\overset{\circ}{q}\left(0\right) = 0$. For both single and double tapered beams we use the following mode shapes (Gorman, 1975; Abdel-Jaber et al., 2008). For the single tapered beam we have:

$$\psi\left(\tilde{x}\right) = \frac{1}{\sqrt{\varsigma}}\left(A_1 J_1\left(2\beta\sqrt{\varsigma}\right) + A_2 Y_1\left(2\beta\sqrt{\varsigma}\right) + A_3 I_1\left(2\beta\sqrt{\varsigma}\right) + A_4 K_1\left(2\beta\sqrt{\varsigma}\right)\right) \tag{34}$$

and for the double tapered beam:

$$\psi\left(\tilde{x}\right) = \frac{1}{\varsigma}\left(A_1 J_2\left(2\beta\sqrt{\varsigma}\right) + A_2 Y_2\left(2\beta\sqrt{\varsigma}\right) + A_3 I_2\left(2\beta\sqrt{\varsigma}\right) + A_4 K_2\left(2\beta\sqrt{\varsigma}\right)\right) \tag{35}$$

where $\varsigma = 1 + (\varepsilon^* - 1)\tilde{x}$ and α is determined using linear frequency-analysis of the system ($\beta^4 = \rho_0 \omega_L^2 A_0 L^4 / E_0 I_0$). Also J_1 and Y_1 are Bessel functions of the first and the second kind, respectively, and I_1 and K_1 are modified Bessel functions of the first and the second kind, respectively. Moreover, A_i's are arbitrary constants that to be found by imposing the boundary conditions of the clamped tapered beam as:

$$\psi(0) = 0,\ \psi'(0) = 0,\ \psi''(1) = 0,\ \left(\tilde{I}\psi'\right)''\Big|_{\tilde{x}=1} = 0 \tag{36}$$

In the following, we present an approximate analytical solution based on the Homotopy analysis method (HAM) and discuss on the effect of material parameters functionality, length-scale parameter and geometrical parameters on the large displacement response of both single (STB) and double (DTB) tapered FG nanobeams.

4 SOLUTION APPROACH: HOMOTOPY ANALYSIS METHOD

In most cases, it is difficult to arrive at an analytical solution for non-linear problems. Perturbation technique is one of the basic methods to analytically solve non-linear problems. In addition to perturbation methods, some non-perturbative methods are developed to be not limited to such constraints. Among several different existing methods, HAM is an effective analytical method for solving non-linear equations. HAM transforms a general non-linear problem into an infinite number of linear problems embedding an auxiliary parameter s. As s varies from 0 to 1, the solution moves from the initial guess to the exact solution. To describe the basic idea of HAM, we consider a general non-linear problem as:

$$\mathbb{N}\left[q(\tau)\right] = 0 \tag{37}$$

in which $\mathbb{N}$ is a general non-linear differential operator and $q(\tau)$ is an unknown function. Let $q(\tau)$ represent an initial guess of the exact solution for $q(\tau)$, $\hbar$ an auxiliary parameter, $H(\tau) \neq 0$ an auxiliary function, and $\mathbb{L}$ an auxiliary linear operator, respectively. Then, using an embedding parameter $s \in [0,1]$, the homotopy function is constructed as (Liao, 2003):

$$\mathbb{N}\left[\Phi(\tau,s), u_0(\tau), H(\tau), \hbar, s\right] = (1-s)\left\{\mathbb{L}\left[\Phi(\tau,s) - u_0(\tau)\right] - s\hbar H(\tau)\mathbb{N}\left[\Phi(\tau,s)\right]\right\} \tag{38}$$

where $\Phi(\tau,s)$ is the primary asymptotic solution. Defining homotopy function as (38), we have a vast number of choices for initial guess, auxiliary linear operator, the nonzero auxiliary parameter and the auxiliary function, which have direct impact on the solution convergence.
Setting the homotopy function zero, the zero-order deformation equation is obtained as:

$$(1-s)\mathbb{L}\left[\Phi(\tau,s) - u_0(\tau)\right] = s\hbar H(\tau)\mathbb{N}\left[\Phi(\tau,s)\right] \tag{39}$$

with $\Phi(0,s) = a$ and $\dfrac{\partial \Phi(0,s)}{\partial s} = 0$. Setting $s = 0$, the zero-order deformation equation becomes:

$$\mathbb{L}\left[\Phi\left(\tau,0\right)-q_0\left(\tau\right)\right]=0 \tag{40}$$

Using (40), it is easy to show that $\Phi\left(\tau,0\right)=q_0\left(\tau\right)$. When $s=1$, the zero-order deformation equation is reduced to:

$$\mathbb{N}\left[\Phi\left(\tau,1\right)\right]=0 \tag{41}$$

which is the same as the non-linear equation (37), provided $\Phi\left(\tau,1\right)=q\left(\tau\right)$. It is observed that as the embedding parameter s increases from 0 to 1, $\Phi\left(\tau,\mathrm{s}\right)$ varies continuously from the initial guess $q_0\left(\tau\right)$ to the exact solution $q\left(\tau\right)$ of (37). Equation (39) is called the zero-order deformation equation. The mth-order deformation derivative is constructed as:

$$q_m\left(\tau\right)=\frac{1}{m!}\frac{\partial^m\Phi\left(\tau,s\right)}{\partial s^m}\bigg|_{s=0} \tag{42}$$

Using Taylors series, $\Phi\left(\tau,s\right)$ and $\omega\left(s\right)$ could be expanded as:

$$\Phi\left(\tau,s\right)=\Phi\left(\tau,0\right)+\sum_{m=1}^{\infty}\frac{1}{m!}\frac{\partial^m\Phi\left(\tau,s\right)}{\partial s^m}\bigg|_{s=0}s^m=\Phi\left(\tau,0\right)+\sum_{m=1}^{\infty}q_m\left(\tau\right)s^m \tag{43}$$

$$\omega\left(s\right)=\omega_0+\sum_{m=1}^{\infty}\frac{1}{m!}\frac{\partial^m\omega\left(s\right)}{\partial s^m}\bigg|_{s=0}s^m=\omega_0+\sum_{m=1}^{\infty}\omega_m s^m \tag{44}$$

with $q_m\left(0\right)=0$ and $\overset{\circ}{q}_m\left(0\right)=0$. Using (41) and (43), we have:

$$q\left(\tau\right)=q_0\left(\tau\right)+\sum_{m=1}^{\infty}q_m\left(\tau\right) \tag{45}$$

To find $q_m\left(\tau\right)$, the higher order deformation equations should be identified. Differentiating (39) m times with respect to s, and then setting s = 0 and finally dividing by m!, higher order approximations of the solution $q\left(\tau\right)$ can be determined by:

$$\mathbb{L}\left[q_m\left(\tau\right)\right]=\Upsilon_m\mathbb{L}\left[q_{m-1}\left(\tau\right)\right]+\hbar H\left(\tau\right)R_m\left[q_1,...,q_{m-1},\omega_0,...,\omega_{m-1}\right];\ \Upsilon_m=\begin{cases}0 & m\le 1\\ 1 & m>1\end{cases} \tag{46}$$

where

$$R_m\left[q_1,...,q_{m-1},\omega_0,...,\omega_{m-1}\right]=\frac{1}{\left(m-1\right)!}\frac{\partial^{m-1}\mathbb{N}\left[\Phi\left(\tau,s\right),\omega\left(s\right)\right]}{\partial s^{m-1}}\bigg|_{s=0} \tag{47}$$

According to (47), the right-hand side of (45) is only dependent on $\left\{q_1\left(\tau\right),q_2\left(\tau\right),...,q_{m-1}\left(\tau\right)\right\}$. Thus, solving (45), q_m is calculated. The mth-order approximation of $q\left(\tau\right)$ is represented by:

$$q(\tau) \approx \sum_{j=0}^{m} q_j(\tau) \tag{48}$$

There are also some techniques to accelerate the convergence of a solution series. Among them, the Pade technique is widely used. The homotopy-Pade technique was proposed by combining the Pade technique with the HAM (Liao, 2003). The corresponding [m, n] Pade approximant for series of (43) about the embedding parameter s, is introduced by:

$$\Phi(\tau,s) = \Phi(\tau,0) + \sum_{m=1}^{\infty} q_m(\tau) s^m = \frac{\sum_{k=0}^{m} A_{m,k}(\tau) s^k}{\sum_{k=0}^{n} B_{n,k}(\tau) s^k} \tag{49}$$

where $A_{m,k}(\tau)$ and $B_{n,k}(\tau)$ are determined by following set of approximations:

$$\left[q_0(\tau), q_1(\tau), q_2(\tau), ..., q_{m+n}(\tau)\right] \tag{50}$$

Setting s = 0, the [m, n] Homotopy-Pade approximant is obtained as:

$$\Phi(\tau,1) = \frac{\sum_{k=0}^{m} A_{m,k}(\tau)}{\sum_{k=0}^{n} B_{n,k}(\tau)} \tag{51}$$

The Homotopy-Pade technique can greatly enlarge the convergence region of the solution series. Besides, Homotopy-Pade approximants often converge faster than solutions calculated by HAM. In many cases, the [m, m] Homotopy-Pade approximants do not depend on the auxiliary parameter $\hbar$. In such cases, even if the corresponding solution series diverge, utilizing the Homotopy-Pade technique results in a convergent series (Liao, 2003).

5 APPLICATION OF HOMOTOPY-PAD'E METHOD TO THE MODEL

Considering the free vibrations, the governing non-linear equation (31) can be recast as follows:

$$\omega^2 \frac{\partial^2 q}{\partial \tau^2} + q + c_4 q^3 + c_5 q^5 = 0 \tag{52}$$

where $\tau = \omega\sqrt{c_2}\hat{t}$. Free oscillation of a system (without damping) represents a periodic motion which could be described by the base functions $\cos(m\tau), \{m = 1,2,...\}$. To satisfy the initial conditions, the following form is considered as the initial guess of $q(\tau)$ for zero-order deformation equation:

$$q_0(\tau) = \tilde{a}\cos(\tau) \tag{53}$$

To produce the Homotopy function, the auxiliary linear operator is chosen as:

$$\mathbb{L}\left[q\left(\tau,s\right)\right]=\omega_0^2\left(\frac{\partial^2 q\left(\tau,s\right)}{\partial\tau^2}+q\left(\tau,s\right)\right) \tag{54}$$

Furthermore, from (50), the non-linear operator is:

$$\mathbb{N}\left[q\left(\tau,s\right),\omega\right]=\omega^2\frac{\partial^2 q\left(\tau,s\right)}{\partial\tau^2}+q\left(\tau,s\right)+c_4q^3\left(\tau,s\right)+c_5q^5\left(\tau,s\right) \tag{55}$$

Whereas the solution should comply with the base functions, the auxiliary function must be selected as $H\left(\tau\right)=1$. Considering the odd non-linearity of the system, it is found that R_m can be expressed by:

$$R_m\left(\tau,\omega_{m-1}\right)=\sum_{n=0}^{m}\Theta_n\cos\left(\left(2n+1\right)\tau\right) \tag{56}$$

To avoid appearing secular terms in the final solution, the coefficient of $\cos\left(\tau\right)$should vanish. Thus, we have $\Theta_1\left(\omega_{m-1}\right)=0$. Solving this equation, $\omega_{m-1}$is obtained. For the first-order approximation of HAM, R_1 is obtained as:

$$R_1=\left(\frac{3}{4}\beta a^3-{\omega_0}^2a+a+\frac{5}{8}\gamma a^5\right)\cos\left(\tau\right)+\left(\frac{5}{16}\gamma a^5+\frac{1}{4}\beta a^3\right)\cos\left(3\tau\right)+\frac{1}{16}\gamma a^5\cos\left(5\tau\right) \tag{57}$$

Thus, $\omega_0$is:

$$\omega_0=\sqrt{\frac{3}{4}\beta a^2+\frac{5}{8}\gamma a^4+1} \tag{58}$$

Solving (46) for m = 1, q_1 is written as:

$$q_1=\hbar\frac{\left(12\beta a^3+16\gamma a^5\right)\cos\left(\tau\right)-\left(12\beta a^3+15\gamma a^5\right)\cos\left(3\tau\right)-\gamma a^5\cos\left(5\tau\right)}{288\beta a^2+240\gamma a^4+384} \tag{59}$$

Moreover, using the coefficient of $\cos\left(\tau\right)$ in R_2, $\omega_1$is:

$$\omega_1=\frac{\sqrt{2}}{192}\frac{a^4\hbar\left(96\beta a^2\gamma+36\beta^2+65\gamma^2a^4\right)}{\left(6\beta a^2+8+5\gamma a^4\right)^{3/2}} \tag{60}$$

Solving (46) for m = 2, we arrive at the following expression for q_2 :

$$q_2\left(\tau\right)=\frac{1}{240C_0}\begin{pmatrix}-\left(30C_1+5C_3+10C_2+3C_4\right)\cos\left(\tau\right)+30C_1\cos\left(3\tau\right)\\+10C_2\cos\left(5\tau\right)+5C_3\cos\left(7\tau\right)+3C_4\cos\left(9\tau\right)\end{pmatrix} \tag{61}$$

in which

$$C_1 = -\frac{a^3\hbar\left(\begin{array}{l}\left(\left(600+615h\right)c_4a^4+480\left(1+\hbar\right)a^2\right)c_5\\+\left(300+320h\right)a^6c_5^2+\left(1+\hbar\right)c_4\left(288c_4a^2+384\right)\end{array}\right)}{192\left(6c_4a^2+5c_5a^4+8\right)} \tag{62}$$

$$C_2 = \frac{a^5\hbar\left(20\gamma^2a^4+\left(\left(24\beta-7h\beta\right)a^2+32\left(1+\hbar\right)\right)\gamma-12h\beta^2\right)}{-64\left(6\beta a^2+8+5\gamma a^4\right)} \tag{63}$$

$$C_3 = \frac{-a^7\gamma\hbar^2\left(72\beta+95\gamma a^2\right)}{4608\beta a^2+6144+3840\gamma a^4} \tag{64}$$

$$C_4 = \frac{5\hbar^2\gamma^2a^9}{4608\beta a^2+6144+3840\gamma a^4} \tag{65}$$

The procedure described in this section is straight-forward and can be followed to higher order of approximations. In next section, it is shown that, $q_{[2,2]}$ and its correspondent frequency $\omega_{[2,2]}$ give very good results compared to the numerical results as well as the experimental data. Thus, we cut the procedure at this step. Whereas $q_{[2,2]}$ is lengthy, it is not reported, however, in the following section, to arrive at an acceptable accuracy we report $q_{[2,2]}$ results (Liao, 2003).

The [1, 1] and [2, 2] Homotopy-Pade approximations of ω and $q\left(\tau\right)$ can be written in the following form (Liao, 2003; Pirbodaghi et al., 2009):

$$\omega_{[1,1]} = \frac{\omega_0\left(\omega_1-\omega_2\right)+{\omega_1}^2}{\omega_1-\omega_2} \tag{66}$$

$$\omega_{[2,2]} = \frac{\left(\omega_3-\omega_4\right){\omega_1}^2+\omega_0\left(\omega_2\left(\omega_3+\omega_4\right)+\omega_1\left(\omega_3-\omega_4\right)\right)+\omega_1\omega_2\left(2\omega_3-\omega_2\right)-{\omega_2}^3-\omega_0\left({\omega_3}^2+{\omega_2}^2\right)}{\omega_4\omega_2-{\omega_3}^2-\omega_4\omega_1+\omega_2\omega_3+\omega_1\omega_3-{\omega_2}^2} \tag{67}$$

$$q_{[1,1]} = \frac{q_0\left(q_1-q_2\right)+{q_1}^2}{q_1-q_2} \tag{68}$$

$$q_{[2,2]} = \frac{\left(q_3-q_4\right){q_1}^2+q_0\left(q_2\left(q_3+q_4\right)+q_1\left(q_3-q_4\right)\right)+q_1q_2\left(2q_3-q_2\right)-{q_2}^3-q_0\left({q_3}^2+{q_2}^2\right)}{q_4q_2-{q_3}^2-q_4q_1+q_2q_3+q_1q_3-{q_2}^2} \tag{69}$$

6 RESULTS AND DISCUSSION

In this Section, in order to investigate the size effects (through the couple stress theory) on the large amplitude vibrations of axially FG beam, numerical results are provided in various material and geometrical properties, e.g., taper ratios, FG parameters and length scale parameters. The nonlinear natural frequencies of the both STB and DTB are calculated and reported in Tables 1-3. A comparison study is performed to verify the reliability of the present work formulation with those reported in Rao and Rao (1988). It is observed that the present work results are in good agreement with those of Rao and Rao (1988). The difference between the present work results and Rao and Rao (1988) results is due to employing the Finite element method in Rao and Rao (1988), while in this work, we developed analytic approximate solutions through assuming a mode shape. To verify the validity of the analytical solution, Table 2 reports the present work results in comparison with the numerical results obtained based on the FFT analysis (with a signal length of 350000 and sampling frequency of 560 Hz). As one may observe, the maximum difference is 1.64%.

STB	$\epsilon^* = 0.2$		$\epsilon^* = 0.4$		$\epsilon^* = 0.6$		$\epsilon^* = 0.8$	
Free tip angle amplitude	Rao and Rao (1988)	Present work	Rao and Rao (1988)	Present work	Rao and Rao (1988)	Present work	Rao and Rao (1988)	Present work
0.01	4.292	4.292 (0.0)	3.934	3.934 (0.0)	3.737	3.737 (0.0)	3.608	3.608 (0.0)
10	4.299	4.301 (0.0)	3.941	3.967 (0.66)	3.744	3.773 (0.77)	3.615	3.644 (0.80)
20	4.317	4.363 (1.02)	3.961	4.065 (2.63)	3.764	3.875 (2.95)	3.636	3.752 (3.19)
30	4.348	4.447 (2.74)	3.994	4.217 (5.58)	3.799	4.039 (6.31)	3.671	3.921 (6.81)
40	4.392	4.556 (2.27)	4.042	4.406 (9.01)	3.848	4.244 (10.29)	3.721	4.134 (11.09)
50	4.452	4.681 (5.14)	4.106	4.626 (12.66)	3.914	4.473 (14.28)	3.788	4.369 (15.34)
60	4.528	4.814 (6.31)	4.188	4.850 (15.80)	3.998	4.711 (17.83)	3.873	4.614 (19.13)

Table 1: Nonlinear natural frequency ratio for a STB and comparison between the present work and Rao and Rao (1988) ($\rho_1 / \rho_0 = E_1 / E_0 = \nu_1 / \nu_0 = 1, l = 0$).

Figs. 3 and 4 depict the effect of changing the mechanical properties along the beam axis, such as density and Young modulus, on the nonlinear frequency ratio with different taper ratio (ε^*) (for both the first and second mode shapes), while the effect of length scale parameter is neglected. To this end, the axially FG beam made of material properties tabulated in Table 4 is considered. In Fig. 3, the nonlinear frequency ratio is plotted as a function of dimensionless amplitude of vibration for different mechanical properties. From Fig. 3 results, it is concluded that for the first mode shape, the nonlinear frequency ratio increases where we encounter an increase in FG parameters (n and m). In contrary to the first mode results, as seen in Fig. 4, we have an opposite trend. Larger values for n and m indicate the conditions in which the equivalent material behavior is more similar to that of the left end of the beam constituent (for both the first and second mode shapes).

STB	$\epsilon^* = 0.2$		$\epsilon^* = 0.4$		$\epsilon^* = 0.6$		$\epsilon^* = 0.8$	
Free tip angle amplitude	FFT	Present work	FFT	Present work	FFT	Present work	FFT	Present work
0.01	4.292	4.292 (0.0)	3.934	3.934 (0.0)	3.737	3.737 (0.0)	3.608	3.608 (0.0)
10	4.306	4.301 (0.12)	3.979	3.967 (0.30)	3.756	3.773 (0.45)	3.654	3.644 (0.27)
20	4.383	4.363 (0.46)	4.103	4.065 (0.93)	3.904	3.875 (0.74)	3.765	3.752 (0.35)
30	4.451	4.447 (0.09)	4.263	4.217 (1.08)	4.021	4.039 (0.45)	3.897	3.921 (0.62)
40	4.584	4.556 (0.61)	4.375	4.406 (0.71)	4.179	4.244 (1.56)	4.071	4.134 (1.55)
50	4.692	4.681 (0.23)	4.647	4.626 (0.43)	4.461	4.473 (0.27)	4.402	4.369 (0.75)
60	4.850	4.814 (0.74)	4.931	4.850 (1.64)	4.766	4.711 (1.15)	4.605	4.614 (0.20)

Table 2: Nonlinear natural frequency ratio for a STB and comparison between the present work and numerical results based on the FFT analysis. Numbers in parentheses are relative differences in percent ($\rho_1 / \rho_0 = E_1 / E_0 = \nu_1 / \nu_0 = 1, l = 0$).

DTB	$\epsilon^* = 0.2$		$\epsilon^* = 0.4$		$\epsilon^* = 0.6$		$\epsilon^* = 0.8$	
Free tip angle amplitude	Rao and Rao (1988)	Present work	Rao and Rao (1988)	Present work	Rao and Rao (1988)	Present work	Rao and Rao (1988)	Present work
0.01	6.196	6.196 (0.0)	5.009	5.009 (0.0)	4.319	4.319 (0.0)	3.855	3.855 (0.0)
10	6.203	6.211 (0.13)	5.017	5.021 (0.09)	4.326	4.334 (0.19)	3.862	3.870 (0.20)
20	6.225	6.236 (0.18)	5.040	5.064 (0.48)	4.349	4.366 (0.40)	3.884	3.906 (0.57)
30	6.261	6.299 (0.61)	5.079	5.137 (1.15)	4.387	4.421 (0.77)	3.921	3.964 (1.10)
40	6.314	6.355 (0.65)	5.135	5.227 (1.8)	4.442	4.495 (1.19)	3.974	4.030 (1.43)
50	6.385	6.470 (1.34)	5.210	5.327 (2.26)	4.515	4.531 (0.36)	4.044	4.117 (1.81)
60	6.475	6.509 (0.52)	5.306	5.375 (1.31)	4.609	4.838 (4.99)	4.134	4.395 (6.31)

Table 3: Nonlinear natural frequency ratio for a DTB and comparison between the present work and Rao and Rao (1988) ($\rho_1 / \rho_0 = E_1 / E_0 = \nu_1 / \nu_0 = 1, l = 0$).

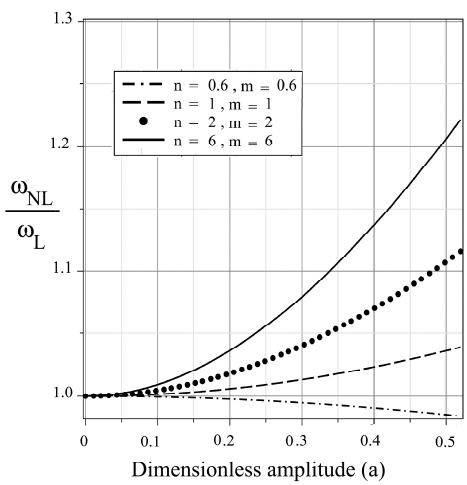

(a)

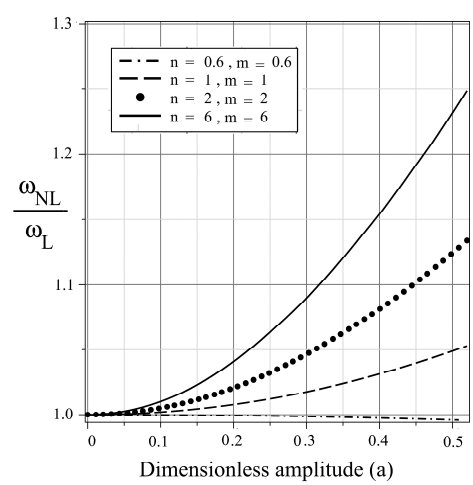

(b)

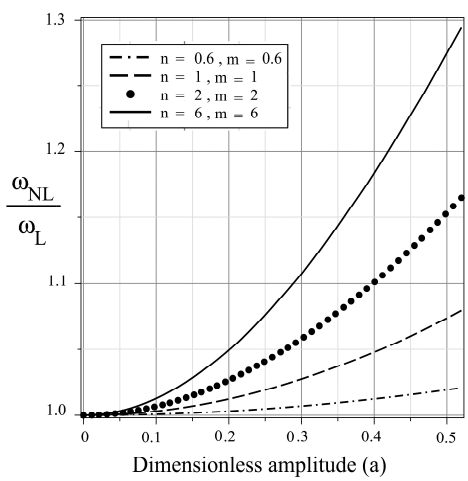

(c)

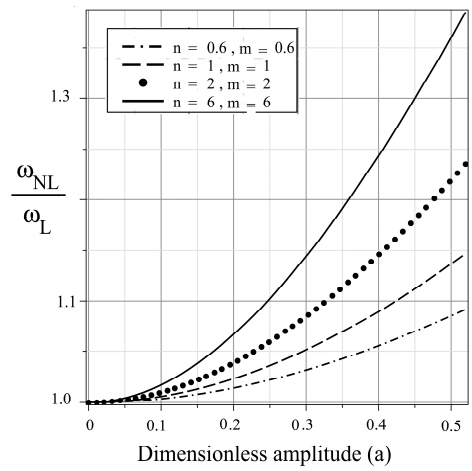

(d)

Figure 3: Nonlinear frequency ratio of the single tapered beam versus free tip nondimensional amplitude for the first mode. a) $\varepsilon^* = 0.2$, b) $\varepsilon^* = 0.4$, c) $\varepsilon^* = 0.6$, d) $\varepsilon^* = 0.8$.

Material	Density [kg/m^3]	Young modulus [GPa]
Steel	7810	212.3
Aluminum	2370	72.6

Table 4: Material properties of constituents in the FG beam.

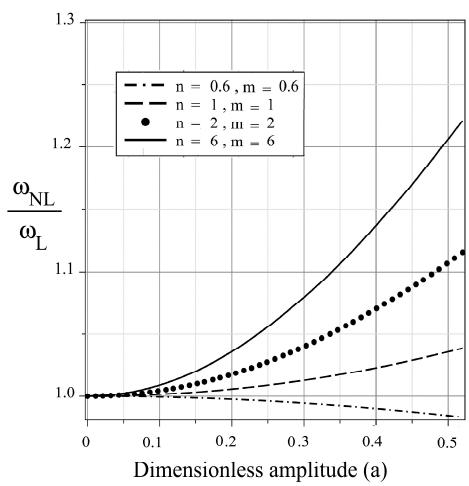

(a)

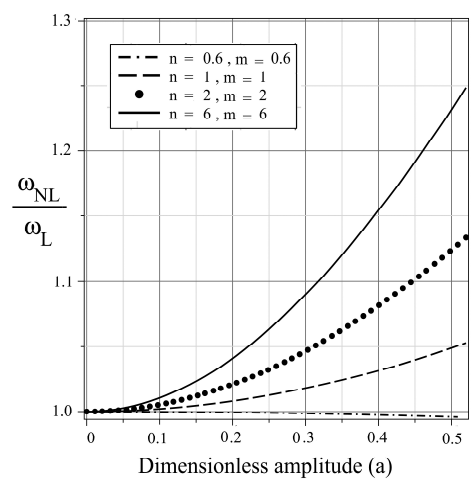

(b)

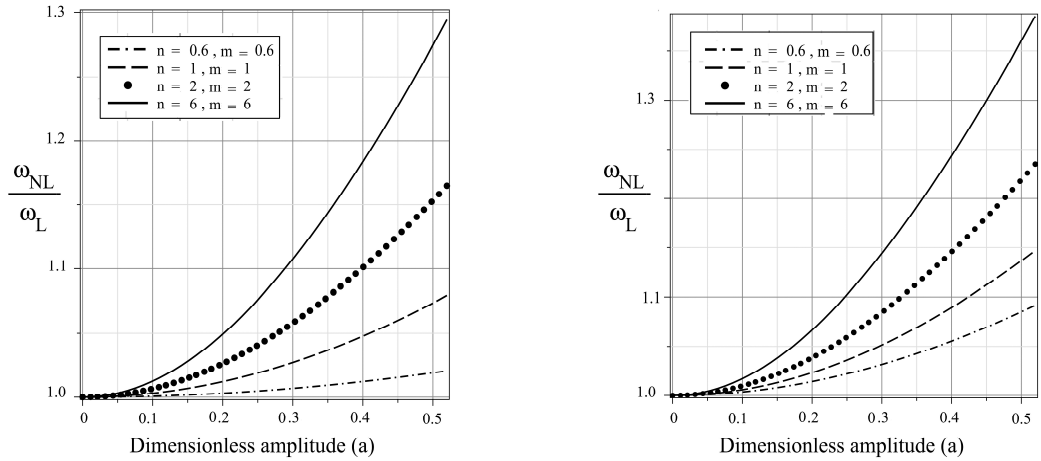

Figure 4: Nonlinear frequency ratio of the single tapered beam versus free tip nondimensional amplitude for the second mode. a) $\varepsilon^* = 0.2$, b) $\varepsilon^* = 0.4$, c) $\varepsilon^* = 0.6$, d) $\varepsilon^* = 0.8$.

In Figs. 5 and 6, the influence of the dimensionless length scale parameter (l / h_0) on the nonlinear natural frequencies of the structure is shown (for both the first and second mode shapes). The nonlinear frequency ratio with dimensionless amplitude is plotted at different values for the mechanical properties (n and m). As observed from Fig. 5, it can be deduced that for the first mode shape, an increase in the length scale parameter decreases the nonlinear frequency ratio, since the increase in the linear frequency is larger than increase in the nonlinear frequency. For the second mode shape (Fig. 6), the trend is reversed.

The effect of the taper ratio on the nonlinear frequency is scrutinized in Figs. 7 and 8 where the nonlinear frequency ratio is plotted versus the dimensionless amplitude in different taper ratios with different mechanical properties (for both the first and second mode shapes). As it can be seen, for the first mode shape, the nonlinear frequency ratio goes up by increasing the taper ratio with different mechanical properties. For the second mode shape, this trend is opposite (Fig. 8).

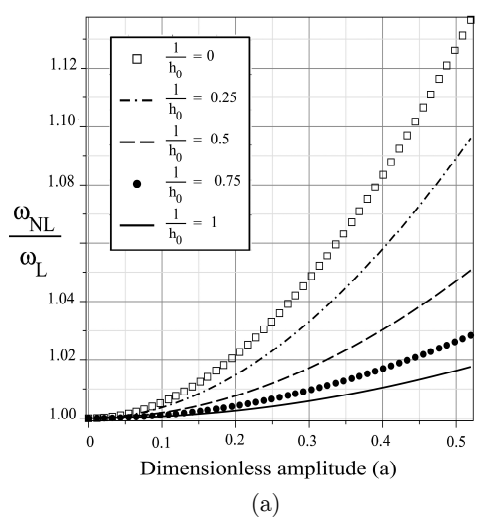

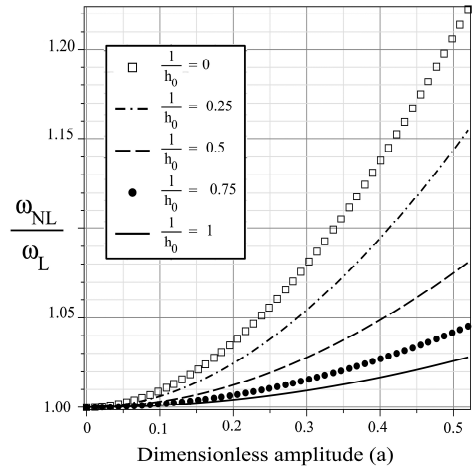

(b)

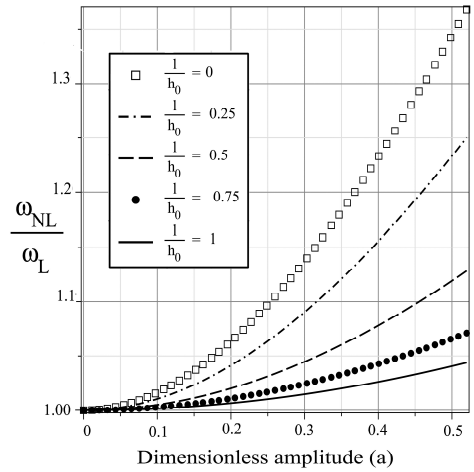

(c)

Figure 5: Nonlinear frequency ratio of the single tapered beam versus free tip nondimensional amplitude for the first mode. n = m = 1, b) n = m = 2, c) n = m = 6.

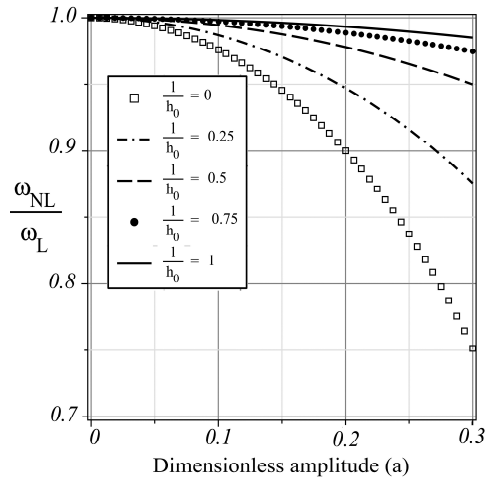

(a)

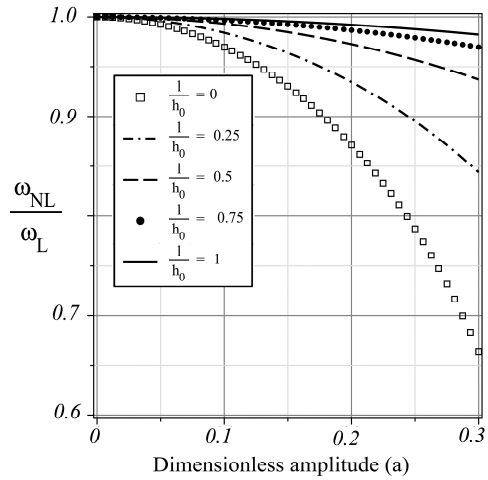

(b)

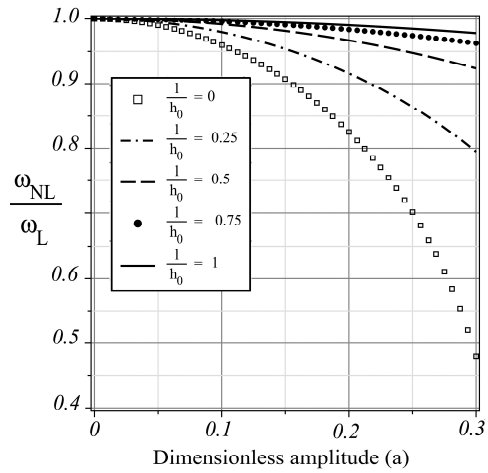

(c)

Figure 6: Nonlinear frequency ratio of the single tapered beam versus free tip nondimensional amplitude for the second mode. n = m = 1, b) n = m = 2, c) n = m = 6.

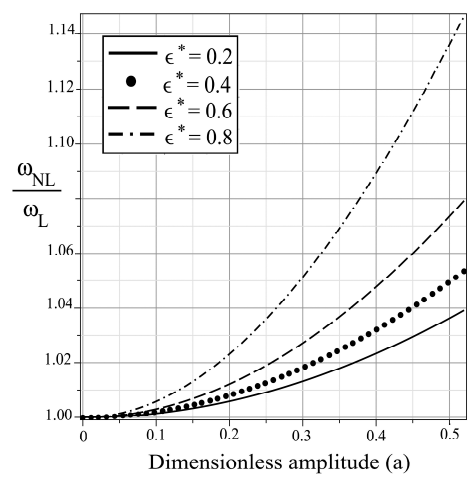

(a)

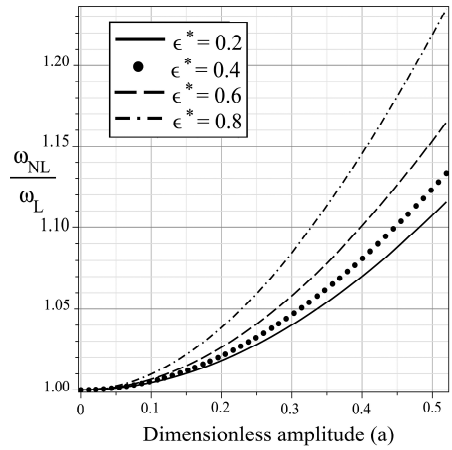

(b)

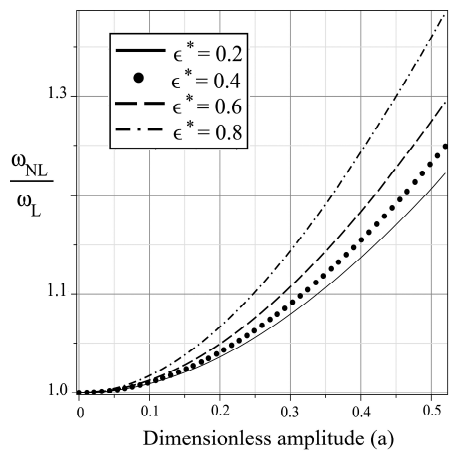

(c)

Figure 7: Nonlinear frequency ratio of the single tapered beam versus free tip nondimensional amplitude for the first mode at different ε^{*}'s . n = m = 1, b) n = m = 2, c) n = m = 6.

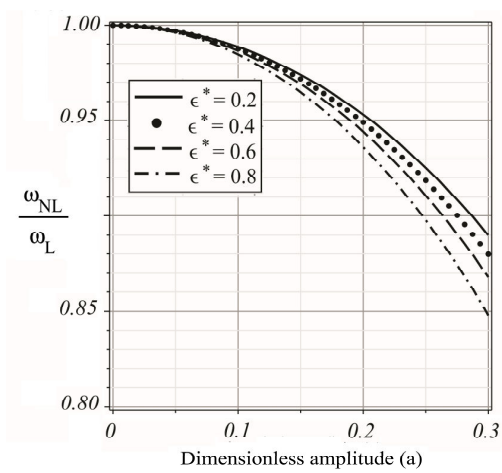

(a)

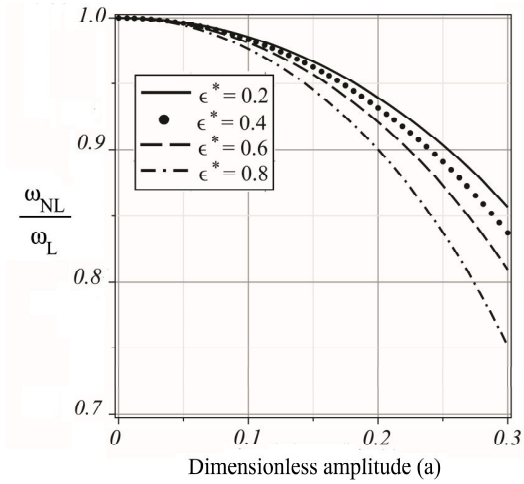

(b)

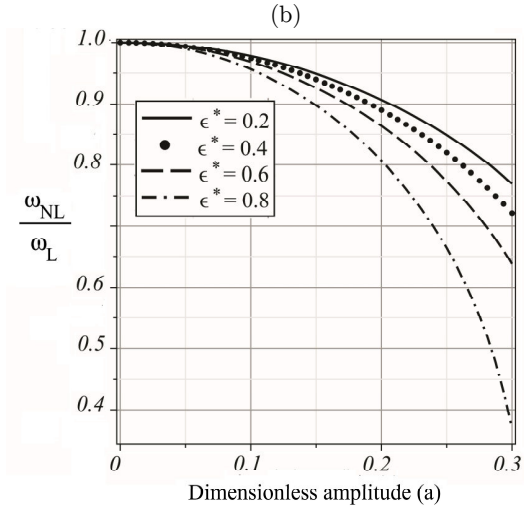

(c)

Figure 8: Nonlinear frequency ratio of the single tapered beam versus free tip nondimensional amplitude for the second mode at different ε^*'s . a) n = m = 1, b) n = m = 2, c) n = m = 6.

7 SUMMARY AND CONCLUSIONS

In this study, Homotopy-Pade analysis method is employed to obtain simple analytical expressions for the non-linear natural frequency and load-deflection relationship of the (single and double) functionally graded tapered nanobeams. The presented expressions are simple, convenient and efficient for the non-linear analysis of the tapered FG beams. Besides, the presented model is valid for a wide range of vibration amplitudes while predictions of the other analytical methods such as perturbation techniques are valid only for the small amplitude vibrations. Comparison between results of the present work and other available data in the literature reveals the accuracy of the presented method. The effects of different parameters such as vibration amplitude and different mode shapes on the natural frequency ratios and displacement response of the FG tapered nanobeams are also investigated. It was shown that increasing the taper ratio, at a given free end initial deflection, increases the non-linear frequency ratio of the single and double tapered beams under the first mode

shape excitation. It was also shown that the beam behaves completely different under the second mode shapes. Moreover, for a given value of a taper ratio, the non-linear natural frequency of a double tapered beam is higher than that of a single tapered beam. Regarding the size-dependency effects, it was observed that in the smaller structures in which these effects are more prominent, fixing the other material parameters, we have larger values for the natural frequency ratios, regardless of the mode shape and/or type of the tapered beam. Moreover, larger values for FG indexes (n and m) indicated that the conditions in which the equivalent material behavior was more similar to that of the left end of the beam constituent (for both the first and second mode shapes regardless of the type of tapered beam).

References

Abdel-Jaber, M., Al-Qaisia, A., Abdel-Jaber, M., Beale, R., (2008). Nonlinear natural frequencies of an elastically restrained tapered beam. Journal of Sound and Vibration 313: 772-783.

Al-Qaisia, A., Hamdan, M., (1999). On the steady state response of oscillators with static and inertia nonlinearities. Journal of sound and vibration 223: 49-71.

Ansari, R., FaghihShojaei, M., Mohammadi, V., Gholami, R., Darabi, M., (2014) Size-dependent vibrations of post-buckled functionally graded Mindlin rectangular microplates. Latin American Journal of Solids and Structures. 11(13): 2351-2378.

Asghari, M., Rahaeifard, M., Kahrobaiyan, M.H., Ahmadian, M.T., (2011). The modified couple stress functionally graded timoshenko beam formulation. Materials and Design 32: 1435-1443.

Baghani, M., (2012). Analytical study on size-dependent static pull-in voltage of microcantilevers using the modified couple stress theory. International Journal of Engineering Science 54: 99-105.

Baghani, M., Fattahi, M., Amjadian, A., (2012). Application of the variational iteration method for nonlinear free vibration of conservative oscillators. Scientia Iranica 19(3): 513-518.

Baghani, M., Jafari-Talookolaei, R.A., Salarieh, H., (2011). Large amplitudes free vibrations and post-buckling analysis of unsymmetrically laminated composite beams on nonlinear elastic foundation. Applied Mathematical Modelling 35: 130-138.

Bazoune, A., Khulief, Y.A., Stephen, N.G., Mohiuddin, M.A., (2001). Dynamic response of spinning tapered timoshenko beams using modal reduction. Finite Elements in Analysis and Design 37: 199 - 219.

Cheng, Y., Yu, Z., Wu, X., Yuan, Y., (2011). Vibration analysis of a cracked rotating tapered beam using the p-version finite element method. Finite Elements in Analysis and Design 47: 825-834.

Fleck, N.A., Muller, G.M., Ashby, M.F., Hutchinson, J.W., (1994). Strain gradient plasticity: Theory and experiment. Acta Metallurgica Et Materialia 42: 475-487.

Fu, Y., Du, H., Huang, W., Zhang, S., Hu, M., (2004). TiNi-based thin films in mems applications: A review. Sensors and Actuators, A: Physical 112: 395-408.

Fu, Y., Du, H., Zhang, S., (2003). Functionally graded TiN/TiNi shape memory alloy films. Materials Letters 57, 2995-2999.

Gorman, D., (1975). Free vibration analysis of beams and shafts. Wiley.

Ke, L.L., Wang, Y.S., (2011). Size effect on dynamic stability of functionally graded microbeams based on a modified couple stress theory. Composite Structures 93: 342-350.

Ke, L.L., Wang, Y.S., Yang, J., Kitipornchai, S., (2012). Nonlinear free vibration of size-dependent functionally graded microbeams. International Journal of Engineering Science 50: 256-267.

Koizumi, M., Niino, M., (1995). Overview of FGM research in japan. MRS Bulletin 20: 19-21.

Kong, S., Zhou, S., Nie, Z., Wang, K., (2008). The size-dependent natural frequency of Bernoulli-Euler micro-beams. International Journal of Engineering Science 46: 427-437.

Koochi A.H., Sedighi, M., Abadyan, M., (2014) Modeling the size dependent pull-in instability of beam-type NEMS using strain gradient theory. Latin American Journal of Solids and Structures 11(10): 1806-1829.

Lam, D.C.C., Yang, F., Chong, A.C.M., Wang, J., Tong, P., (2003). Experiments and theory in strain gradient elasticity. Journal of the Mechanics and Physics of Solids 51: 1477-1508.

Lee, Z., Ophus, C., Fischer, L., Nelson-Fitzpatrick, N., Westra, K., Evoy, S., Radmilovic, V., Dahmen, U., Mitlin, D., (2006). Metallic nems components fabricated from nanocomposite al-mo films. Nanotechnology 17: 3063-3070.

Liao, S., (2004). On the homotopy analysis method for nonlinear problems. Applied Mathematics and Computation 147: 499-513.

Liao, S.J., (2003). Beyond Perturbation: Introduction to Homotopy Analysis Method. Chapman Hall/CRC.

McFarland, A.W., Colton, J.S., (2005). Role of material microstructure in plate stiffness with relevance to microcantilever sensors. Journal of Micromechanics and Microengineering 15: 1060-1067.

Mindlin, R.D., Eshel, N.N., (1968). On first strain-gradient theories in linear elasticity. International Journal of Solids and Structures 4: 109-124.

Pirbodaghi, T., Hoseini, S.H., Ahmadian, M.T., Farrahi, G.H., (2009). Duffing equations with cubic and quintic nonlinearities. Computers and Mathematics with Applications 57: 500-506.

Rao, B.N., Rao, G.V., (1988). Large amplitude vibrations of a tapered cantilever beam. Journal of Sound and Vibration 127: 173-178.

Rezaiee-Pajand M., Yaghoobi, M., (2014). An efficient formulation for linear and geometric non-linear membrane elements. Latin American Journal of Solids and Structures. 11(6): 1012-1035.

Sadeghi, H., Baghani, M., Naghdabadi, R., (2012). Strain gradient elasticity solution for functionally graded micro-cylinders. International Journal of Engineering Science 50: 22-30.

Saffari, H., Rahgozar, R., Jahanshahi, R., (2008). An efficient method for computation of effective length factor of columns in a steel gabled frame with tapered members. Journal of Constructional Steel Research 64: 400-406.

Schulz, U., Peters, M., Bach, F.W., Tegeder, G., (2003). Graded coatings for thermal, wear and corrosion barriers. Materials Science and Engineering: A 362: 61-80.

Shahba, A., Attarnejad, R., Marvi, M., Hajilar, S., (2011). Free vibration and stability analysis of axially functionally graded tapered timoshenko beams with classical and non-classical boundary conditions. Composites Part B: Engineering 42(4): 801-808.

Stolken, J.S., Evans, A.G., (1998). A microbend test method for measuring the plasticity length scale. Acta Materialia 46: 5109-5115.

Witvrouw, A., Mehta, A., (2005). The use of functionally graded poly-sige layers for MEMs applications. Materials Science Forum 492-493, 255-260.

Yang, F., Chong, A.C.M., Lam, D.C.C., Tong, P., (2002). Couple stress based strain gradient theory for elasticity. International Journal of Solids and Structures 39: 2731-2743.

Yoshiyuki, Y., (1968). An intrinsic theory of a cosserat continuum. International Journal of Solids and Structures 4: 1013-1023.